Journal of Loss Prevention in the Process Industries 52 (2018) 113–124

Contents lists available at ScienceDirect

Journal of Loss Prevention in the Process Industries

journal homepage: www.elsevier.com/locate/jlp

Numerical investigation of bund overtopping under storage tank failure events

Damian E. Ramajo[a,b,*], Santiago F. Corzo[a], Santiago Marquez Damian[a,c], Juan M. Gimenez[a,b], Norberto M. Nigro[a,b]

[a] CIMEC Centro de Investigación de Métodos Computacionales (UNL, CONICET), Santa Fe, Argentina
[b] UNL Universidad Nacional del Litoral, Argentina
[c] UTNRSF Universidad Tecnológica Nacional Regional Santa Fe, Argentina

ARTICLE INFO

Keywords:
Tank failure
CFD
Bund overtopping
Volume of fluid method

ABSTRACT

In this paper computational fluid dynamics simulations (CFD) were carried out in order to investigate the efficiency of bund designs and top wall deflectors (breakwaters) under several tank failure modes. Investigation was performed over laboratory scale configurations, some of them were also experimentally studied. Simulations were performed using the Volume of Fluid (VOF) method and literature data were used for assessing the solver prior to investigate the different bund designs. Numerical and experimental results agreed, showing the suitability of numerical methods to predict overtopping. The amount of liquid lost showed a low dependency with the containment shape (square, circular or rectangular), but a high one with the bund height. On the contrary, the use of breakwaters showed to be a suitable and very efficient way to reduce liquid loss, although inducing significant extra mechanical efforts over the bund walls.

1. Introduction

The tanks to store hazardous liquids are usually surrounded by a retaining wall or bund generally made of sloped earth or concrete high-collar bunds. The purpose of their is to retain any spillage of the stored liquid which may occur. These secondary containments may have a variety of configurations (square, circular, rectangular), capacities and shapes of bunds. In its guidance on the storage of flammable liquids in tanks, the Health Safety Executive (Great Britain) states that "a bund capacity of 110% of the largest storage vessel will normally be sufficient" and that "the bund should have sufficient strength to contain any spillage" (Thyer et al., 2002).

Although the bunds that surround the storage tanks are commonly over-dimensioned to contain up to 110% of the tank capacity, it is well established that they will not totally avoid liquid loss under severe tank failures (Clark et al., 2001). It has been corroborated by experimental tests as well as real vessel failures. Experiments carried out with a model storage tank inside a 110% bund capacity have shown that, even for slow tank draining (over a period of 30s), the bund is overtopped in almost every case (ref: in HSE Contract Research Report 405/2002). Atherton (Atherton and Ash, 2007) has reported that under severe failures a significant amount of liquid could still overtop bunds designed to retain 200% of the tank total capacity.

Failures can be attributed to a number of causes including human error, inappropriate or poor maintenance, loss of wall thickness by corrosion, vapor ignition, differential settlement, earthquakes, lightening strikes, hurricanes, flood damage and over-pressurization. Such incidents have highlighted the need for the proper assessment of potential risks and the requirement for suitable methods of mitigation. Chang and Lin (2006) reviewed more than 240 accidents along the world and found that 74% of accidents occurred in petroleum refineries and oil storage terminals, and 85% of the accidents involved fire and explosions. The main failure causes were by lightning (33%) and human errors including poor operations and maintenance (30%). The rest was consequence of equipment failure, sabotage, crack and rupture, leak and line rupture, static electricity and open flames. The structural collapse of oil storage tanks is frequently the result of combined and synergistic interaction of mechanical stress and corrosion reactions. Cracks are generally initiated by corrosion, although failure is consequence of the propagation of the cracks caused by stresses concentration (Kim et al., 2009).

Evidently, the more severe the failure the more the overtopping. These catastrophic tank failures are unusual and consequently the risk related to such events is estimated to be lower than 5×10^{-6} per tank

* Corresponding author. CIMEC Centro de Investigación de Métodos Computacionales (UNL, CONICET), Santa Fe. Argentina.
E-mail address: dramajo@santafe-conicet.gov.ar (D.E. Ramajo).
URL: http://www.cimec.org.ar (D.E. Ramajo).

https://doi.org/10.1016/j.jlp.2018.01.006
Received 14 June 2017; Received in revised form 15 December 2017; Accepted 9 January 2018
Available online 17 February 2018
0950-4230/

List of symbols

γ	Phase fraction []
$\mathbf{U}$	Velocity [m/s]
p	Pressure [Pa]
t	Time [s]
ρ	Density [kg/m^3]
μ	Dynamic viscosity [Pa s]
τ	Stress tensor [N/m^2]
I	Identity matrix []
k	Turbulent kinetic energy [m^2/s^2]
ε	Turbulent dissipation rate [m^2/s^3]
σ	Surface tension coefficient [N/m]
$\mathbf{g}$	Gravitational acceleration [m/s^2]
$\mathbf{S}$	Mean rate stress tensor [1/s]
$\mathbf{x}$	Position vector [m]
V_c	Containment volume capacity [m^3]
V_t	Initial stored tank Volume [m^3]
V_l	Volume of the liquid leaving the containment [m^3]
R_v	Containment capacity ratio. $R_v = V_c/V_t$ []
Q	Overtopping fraction ($Q = 100[V_t - V_l]/V_t$) [%]
D_s	Characteristic grid size [m]
N_t	Amount of grid elements []
y	Distance from the tank center to the bund [m]
z	Minimum distance from the tank wall to the bund [m]
d	Distance from the tank wall to the bund corner [m]
H	Liquid column height [m]
h	bund height [m]
θ	Containment slope angle [°]
R	Tank radius [m]
r_{eq}	Equivalent tank to bund distance [m]
M	Momentum [Nm]
F	Force [N]

Subscripts:

l	Liquid phase
g	Gas phase
r	Relative value
t	Turbulent
eff	Effective

Acronyms:

BW	Breakwater
CFD	Computational Fluid Dynamics
GAMG	Geometric Algebraic Multi-Grid
MULES	Multid. Univ. Limiter with Explicit Sol
RANS	Reynolds-averaged Navier-Stokes
SGS	Symmetric Gauss-Seidel
VOF	Volume Of Fluid

year (Thyer et al., 2002). Despite this, the consequences for workers and the environment can be very severe.

Although total tank failure is a very unlikely event, the probability for that scenarios grows with the lack of control and maintenance. Such failures have occurred in the USA, Greece, Lithuania and Argentina, among others. There have been more than 100 major incidents involving storage facilities globally in the last 20 years and the worst that has ever befallen took place at the Buncefield Oils Storage Deposit in Hertfordshire in 2005. It has been regarded as the largest explosion in Europe since the Second World War (Atherton and Ash, 2007). In 1988 a tank spilled more than 14.000 m^3 of oil in the USA. The tank failed during filling because of a crack developed near the tank base, which rapidly propagated vertically to the top in less than a second (Mesloh et al., 1988). More recently, in 2015 in Argentina, an oil wash tank failed in similar conditions spilling 1.700 m^3 of oil and water.

Modelling of asymmetric modes of failure or "jetting failures" has been undertaken over a number of tanks and bunds geometries, and the results to date indicate that the levels of overtopping and the magnitudes of the dynamic pressures are significantly high enough to cause concern.

The structural integrity of the bund as a result of the dynamic pressures involved is of possible greater significance. Failures, which can occur as a result of a damaged pipe or valve connection, or even the partial remotion of a small section of a tank wall, can be particularly problematic. The issue here is the magnitude of the dynamic pressure of the fluid hitting the wall combined with the duration of the impact, which will be more powerful than any normal static pressure. In the instance of earthen dykes, there is a high probability that the earth would be eroded, resulting in the total loss of secondary containment. On the other hand, in the case of concrete walls, the impact could result in the loss of integrity of the structure, removing part of the bund or the breakwaters. Precursor studies (Cuperus, 1980, Rouzsky, 1983; Baldwin, 1983; Bombard and Vehlin, 1983) on high-collar bunds indicated that the hydrodynamic loading near the base of a bund could be between three and six times higher than the expected from hydrostatic loads (Thyer et al., 2002).

Catastrophic tank failures could become worse if more than one tank is housed in the secondary containment. In this case, the hydrodynamic load could easily produce dents or even demolish the adjacent tanks (Thyer et al., 2002).

Assuming that the bund remains intact in the event of a tank failure, a fraction of the stored liquid will inevitably be lost due to the energy of fluid wave or jet impacting against the secondary containment. Estimations made from actual incidents have shown that between 25% and 50% of the original contents were lost. Furthermore, the losses over vertical bund walls without breakwaters, earthen dykes or constructed embankments can be even higher. The more important factor is not the volume of the liquid spill, but the rate at which it is spilled: fast spills can pass over the top of most containment dykes.

To date, few researchers have dedicated to perform experimental tests, mostly reporting the overtopping and sometimes also the mechanical efforts over the bund. Some tests have been related to total failures (Atherton and Ash, 2007), (Atherton et al., 2004) whereas others focused on particular leakage scenarios based on real accidents (Pettitt and Waite, 2003).

The influence of the bund shape and the slope angle of embankments was firstly experimentally investigated by Greenspan et al. (Greenspan and Young, 1978), and subsequently by Clark and Savery (1993) and Law and Johnskareng (1994) in the Imperial College. They found that the lower overtopping was obtained with concave curved bunds followed by vertical bunds (90°) and finally by 60° and 40° inclined bunds. They also found that there is a linear dependency among the overtopping factor and the bund to tank distance.

Perhaps the pioneer works combining numerical and experimental tests were from the Imperial College of London in the 80's. These precursor researchers showed the dependence of the overtopping with the bund height and bund distance from the tank. Nonetheless, they only considered complete failures with vertical bunds without breakwaters.

Much of the numerical investigation has been made using the shallow water method. The most relevant work is from Ivings and Webber (2007), Ivings and Webber (Webber and Ivings, 2010) and SreeRaj (2008). The first ones investigated the response of square containments made of vertical bunds under complete failure, partial leakage from the tank bottom side, and small and big holes. SreeRaj

used Computational Fluid Dynamics (CFD) through the shallow water method to simulate the wave effects and to quantify the overtopping and overpressure on bunds. He found that the maximum pressure is on the corners. Moreover, the study looked further into various bund design options and concluded that the increase of the bund height will reduce, although not completely eliminate overtopping. On the other hand, the use of inclined breakwaters attachment on the top of the bunds considerably reduced overtopping.

From a depth literature review, it is concluded that the available information was almost exclusively obtained from laboratory scale test facilities. However, the applicability of the small-scale test studies to industrial scale installations or multiple tank configurations is still uncertain; arguments based on scaling of roughness suggest that laboratory scale models may underestimate the true overtopping fraction (Thyer et al., 2002). Although Thyer et al. did not provide results, they concluded that overtopping is higher for laboratory scale tests than for large scale installations. Recently, Zhang et al. (2017) carried out experimental tests for laboratory scale (tank radius 230 mm) and field scale configurations (tank radius 516 mm) showing that for square straight vertical bunds such as the currently studied, the laboratory and field tests results were in very good agreement for a wide range of containment capacity ratios ($R_v = V_c/V_t$). On the other hand, for square curved bunds, the overtopping results for laboratory tests were significantly higher than for field tests. From our point of view, the roughness as well as the interfacial effects have a marginal or second order incidence because the dam break phenomenon is mainly dominated by inertial effects.

Some researchers have proposed correlations to estimate overtopping (Q) based on theoretical modelling and shallow water methods as well as experimental data obtained from total collapse tests with square containments without breakwaters. Clark et al. (2001) first proposed the following expression:

$$Q = exp\,[-P(h/H)], \tag{1}$$

where h is the bund height, H is the tank height and P is a factor depending on the slope angle θ of the containment. $P = 3.89$, 2.43, or 2.28 for 90°, 60° and 30°, respectively. Later, Thyer et al. (2002) developed a quite more complex relationship:

$$Q = A + B.\ log(h/H) + C.\ log(r_{eq}/H), \tag{2}$$

where r_{eq} is an equivalent secondary containment radius, A, B and C are 0.044, −0.264 and −0.116 for $\theta = 90°$; 0.287, −0.229 and −0.191 for $\theta = 60°$ and 0.155, −0.360 and −0.069 for $\theta = 30°$. The last expression not only accounts for the bund height h and bund inclination θ but also for the equivalent radius r_{eq}. Hence, this considers all the main containment characteristics, although it does not consider the presence of breakwaters.

The present work is addressed to give guidelines to design secondary bund containments to completely avoid or large reduce overtopping also keeping the mechanical integrity of the bund. The following issues are evaluated and discussed:

a) The nature of the tank failure (total collapse, small holes, vertical and horizontal cracks).
b) The shape of the secondary containment (circular, square or rectangular)
c) The relation between the bund and tank heights
d) The distance between the tank and the bund
e) The influence of using breakwaters

2. Mathematical background

The mathematical background presented below is based on the Volume Of Fluid (*VOF*) solver interFoam from OpenFOAM-2.4© (Open Field Operation and Manipulation). The *VOF* method was proposed by Hirt and Nichols (1981) and started a new trend in multiphase flow simulation. It relies on the definition of an indicator function, which allows knowing whether the computational cell is filled by one fluid, by the other or by a mix of them. This is accomplished by the phase fraction γ, which can take values within the range $0 \le \gamma \le 1$, being the values of zero and one associated to regions where only one phase is present. e.g., $\gamma = 0$ for gas and $\gamma = 1$ for liquid. The method was described in depth by Ubbink (1997) and Rusche (2002), but a concise explanation was given by Berberovic et al. (2010). One of the critical issues using *VOF* is the conservation of the phase fraction γ. This is specially the case in flows with high density ratios, where small errors in γ may lead to significant differences in calculations of physical properties. Furthermore, accurate calculation of the phase fraction distribution is crucial to get a thin and smooth interface to properly evaluate the interface curvature, being the last one required for the determination of the surface tension force and the corresponding pressure gradient through the interface. Finally, the interface region between two phases is typically smeared over a few grid cells and is therefore highly sensitive to grid resolution. Here, we give an overview of the mathematical background concerning *VOF*. In the conventional *VOF* method, the transport equation for an indicator function representing the volume fraction of one phase is solved simultaneously with the continuity and momentum equations. Therefore, it is not a simple task to assure boundedness and conservativeness of the phase fraction.

The Reynolds Average Navier-Stokes (RANS) equations for unsteady incompressible flow are written in terms of the assembled velocity $\overline{U}$. Then, the continuity equation (3), the indicator transport equation (4) and the momentum transport equation (5) are the following:

$$\nabla\cdot\overline{U} = 0 \tag{3}$$

$$\frac{\partial\gamma}{\partial t} + \nabla\cdot(\gamma\overline{U}) + \nabla\cdot(\gamma\overline{U_r}(1-\gamma)) = 0 \tag{4}$$

$$\begin{aligned}&\tfrac{\partial(\rho\overline{\mathbf{U}})}{\partial t} + \nabla\cdot(\rho\overline{\mathbf{U}}\,\overline{\mathbf{U}}) - \nabla\cdot(\mu_{eff}\nabla\overline{\mathbf{U}}) =\\ &-\nabla\overline{p_d} - \mathbf{g}\mathbf{x}\cdot\nabla\rho + \nabla\cdot(\mu_{eff}(\nabla\overline{\mathbf{U}})^T)\\ &+\sigma\kappa\nabla\gamma\end{aligned} \tag{5}$$

$\overline{U}$ is the velocity field shared by the two fluids throughout the flow domain and γ is the phase fraction. ρ is the density, p_d a modified pressure, $\mathbf{g}$ the gravitational acceleration, σ is the surface tension coefficient and κ is the local curvature of the free surface. The last term in Equation (5) represents the surface tension force and was proposed by Brackbill (Brackbill et al., 1992). The curvature κ is defined as:

$$\kappa = -\nabla\cdot\left(\frac{\nabla\gamma}{|\nabla\gamma|}\right) \tag{6}$$

In Equation (5) the viscous stress tensor (laminar) and the Reynolds stress tensor (turbulence) were combined to write the transport equation in terms of and effective viscosity $\mu_{eff} = \mu + \mu_t$, being μ the dynamic viscosity and μ_t the turbulent viscosity.

In order to keep the interface thickness as small as possible, an aditional compression term is added to the γ equation (Eq. (4)), which is related in terms of the relative velocity $\mathbf{U_r} = \mathbf{U_l} - \mathbf{U_g}$. Similarly, the $\overline{U}$ is proportional to the phase fraction γ and the phase velocities:

$$\overline{U} = \gamma\mathbf{U_l} + (1-\gamma)\mathbf{U_g} \tag{7}$$

where $\mathbf{U_l}$ and $\mathbf{U_g}$ are the liquid and the gas velocities respectively.

In the *VOF* formulation two immiscible fluids are considered as one fluid throughout the domain and its physical properties are calculated as weighted averages based on the liquid volume fraction. Thus, mixed properties are only found across the interface,

$$\rho = \gamma\rho_l + \rho_g(1-\gamma) \quad \mu = \gamma\mu_l + \mu_g(1-\gamma) \tag{8}$$

Finally, the modified pressure p_d is introduced to simplify the boundary conditions formulation:

$$p_d = p - \rho \mathbf{g}\cdot\mathbf{x} \tag{9}$$

where $\mathbf{x}$ is the position vector.

To close the equations system, the turbulent viscosity μ_t is obtained by assuming a relationship between the turbulence intensity (velocity fluctuations) and a characteristic length scale L through the Eddy viscosity theory as follows:

$$\mu_t = C_\mu \rho \mathbf{U}' L = C_\mu \rho \frac{k^2}{\varepsilon} \tag{10}$$

where k is the turbulent kinetic energy and ε is the turbulent dissipation rate. In this paper, the standard RANS k-ε model (Launder and Spalding, 1974) with standard wall law was chosen to obtain the turbulent viscosity through two additional transport equations:

$$\frac{\partial \rho k}{\partial t} + \nabla\cdot(\rho k \overline{U}) = \nabla\cdot\left(\frac{\mu_t}{\sigma_k}\nabla k\right) + 2\mu_t S\colon S - \rho\varepsilon \tag{11}$$

$$\frac{\partial \rho \varepsilon}{\partial t} + \nabla\cdot(\rho \varepsilon \overline{U}) = \nabla\cdot\left(\frac{\mu_t}{\sigma_\varepsilon}\nabla \varepsilon\right) + C_{1\varepsilon} 2\frac{\varepsilon}{k}\mu_t S\colon S - \rho C_{2\varepsilon}\frac{\varepsilon^2}{k} \tag{12}$$

The model constants are by default $C_u = 0.09$, $C_{1\varepsilon} = 1.44$, $C_{2\varepsilon} = 1.92$, $\sigma_k = 1.0$ and $\sigma_\varepsilon = 1.3$.

3. Model settings

Simulations were carried out in local parallel computing in a desktop computer (i7 4790 3.6 GHz 4-cores). This low computational resource was enough to perform accurate simulations with relatively coarse grids in short time (few hours or days depending on the mesh size). The main setting parameters are listed in Table 1. Taking advantage of symmetry, a fraction of the full geometries were simulated. Fig. 1 shows the test configurations and the main geometrical parameters for circular (top) and square (bottom) containments. Such as in the experimental tests, only a fraction of the full geometry was simulated (1/4 for square and 1/6 for circular). The boundary conditions were no slip (zero *fixedValue* for velocity) for the floor and the bund walls and *symmetry* for the lateral patches. For the bounding patches, a null total pressure for p_d (*totalPressure*) and inlet/outlet condition (*pressureInletOutletVelocity*) for U was fixed.

Adjustable time step with a maximum Courant number limited to one was chosen, guaranteeing stability as well as accuracy. Simulations ran until sloshing was not enough to produce overtopping.

4. Results and discussion

In this section the results are organized in order to point out the key aspects listed in the introduction section.

4.1. Computational model assessment

In spite of the fact that the possible failure scenarios are infinite, the more likely failure configuration was chosen for model assessment by comparing the numerical results with experimental data by Atherton (Atherton and Ash, 2007). In this sense, total collapse tanks in circular and square secondary containments with vertical bunds (without breakwaters) were chosen.

For both tests the tank radius R was 300 mm, the tank height was 600 mm and the bund height was 120 mm. The distance y from the tank center to the bund was 624 mm and 704 mm for the square and circular tests, respectively. For both cases, the ratio between the tank storage volume and the containment volume $R_v = V_c/V_t$ was 1.1, which is the minimum recommended for design.

For the square case, the computational domain was a box of 1124 mm in wide × 1124 mm in depth × 900 mm in height. In this case, four structured meshes with mean grid cell sizes (D_s) of 20 mm, 10 mm, 7.5 mm and 5 mm were tested to achieve grid independence. Refinement was performed by reducing the grid elements homogeneously. In all cases the grids were built with Cartesian hexahedral cells with aspect ratio close to one. For the circular case, only two meshes were considered: the coarsest one with a mean cell size of 7.5 mm (similar than mesh 3), and the finest one with a cell size of 5 mm (similar than mesh 4). Table 2 resumes the grid parameters.

From the available experimental data, two main parameters were chosen for comparison: the impact time at the bund and the overtopping fraction. Additional data, such as the pressure probes at the wall corner, were not considered for comparison because the geometry and location of probes were ambiguously reported, whereas CFD results showed to be extremely sensitive to the probe locations.

The numerical and experimental data are compared in Table 3. As expected, the agreement between CFD and experimental data improved with the grid refinement. The best agreement was found in the square configuration, and for the finest grid (Mesh 4_s) the overtopping error was less than 3%. On the other hand, for the circular configuration and the finest grid, the error was 4.6%. It should be remarked the agreement between experimental and numerical results, which was due to an appropiated 3D modelling. Zhang et al. (2017) have recently carried out simulations of circular containments using 2D axisymmetric models with VOF and RNG k-ε largely underestimating the overtopping (discrepancies grew up to 23% for $R_v = 1.1$).

The CPU time was also included in the table to evaluate the relation between the computational cost and the accuracy of the solution. The time required for solving 4 s of real time with the second grid was 20 times greater than the required with the first one, whereas, the calculation with the third grid demanded 10 more times computational effort than with the second grid.

Fig. 2-a shows the temporal distribution of the liquid inventory inside the secondary containment. As mentioned above, the time for the first impact of the water wave was around 0.35s and caused the largest inventory loss. After the first impact, the wave returned to the tank inducing a high sloshing wave that subsequently impacted the bund around 2.2s again, which slightly increased the total liquid loss. The inventory evolution curves were almost the same for the four grids and the first and second impact times were also similar.

Fig. 3 shows the liquid distribution for the four grids. Significant differences could be identified by comparing the first three cases, whereas very similar solutions were observed between grids 3 and 4. The same conclusions were found by analyzing the quantitative results in Table 3. However, it is noticeable the increment in the computational time required for solving the finest grid. Therefore, the grid 3 was chosen for performing the next simulations.

Table 1
Solvers and settings description.

Term	OpenFOAM terminology	Method/Scheme
$\frac{\partial}{\partial t}$	CrankNicolson 1	Crank-Nicolson scheme
$\nabla\cdot()$	Gauss LinearUpwind	Second order,upwind-biased
$\nabla\cdot(\nabla..)$	Gauss Linear corrected	Second order
$\nabla\mathbf{U}$	Cell Limited Gauss Linear 1	Cell-value linear limit.
$\nabla..$	Face Limited Gauss Linear 1	Face-value linear limit.
$\nabla(..)_f$	Linear corrected	Linear
γ-eqn.	MULES	–
MULES high order	Vanleer	TVD Vanleer
MULES low order	upwind	Upwind
Eqn.	Solver	Abs. tol.
γ	MULES	1×10^{-8}
p	GAMG	1×10^{-8}
U,k,ε	smoothSymGasussSeidel	1×10^{-8}
PIMPLE	Momentum pred.	nOc, nIc, nNonOc
Square test	yes	1, 5, 0
Circular test	yes	1, 5, 1
MULES	Solver	Cor, subcyclin OutCor
	smooth SymGaussSeidel	1, 1, yes

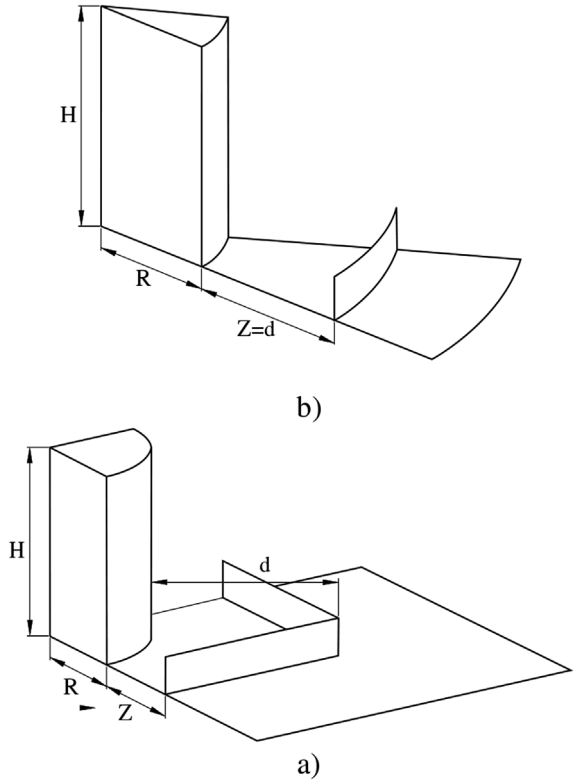

Fig. 1. Square and circular bund tests. a): sketch of the square test. b): sketch of the circular test.

Table 2
Grid parameters for the square and circular cases.

	N_x	N_y/N_{cir}	N_z	N_T	$D_s\,[mm]$
Square domains					
Mesh 1_s	56	56	45	141,120	20
Mesh 2_s	108	108	86	1,003,104	10
Mesh 3_s	162	162	129	3,385,476	6.9
Mesh 4_s	216	216	176	8,211,456	5
Circular domains					
Mesh 1_c	120	80	120	1,044,600	7.5
Mesh 2_c	241	120	180	3,391,380	5.0

Table 3
Comparison between numerical and experimental data. (* time up to the first second of simulation).

	Q [%] (%error)	Arrival time [sec]	CPU time [hrs]
Square test			
Experiment	**48.5**	**0.35**	–
Mesh 1_s	51.48 (%6.0)	0.32	0.39
Mesh 2_s	50.79 (%4.6)	0.32	7.77
Mesh 3_s	50.02 (%3.02)	0.33	61.55
Mesh 4_s	49.89 (%2.76)	0.33	119*
Circular test			
Experiment	**47.66**	**0.22**	–
Mesh 1_c	52.18 (%9.5)	0.25	51.58
Mesh 2_c	50.79 (%4.6)	0.26	102*

Fig. 4 shows the solution for the circular bund tests at four times for both grids. Results were very similar. It was noticeable the maximum height reached by the wave at $t = 0.6\,s$.

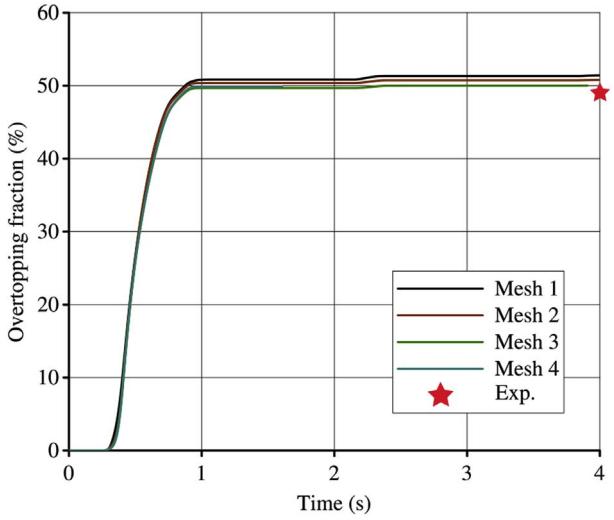

Fig. 2. Inventory distribution for square bund test.

4.2. Nature of the tank failure

The failure modes in the event of a real tank collapse may be highly complex and involve the interaction between fracture propagation and fluid dynamic effects. For a total collapse, such as the currently considered, the main assumption is that the cracks propagate much faster than the fluid motion. Thus, the tank suddenly losses integrity and collapses delivering all the stored fluid in all directions.

The present section evaluates the total collapse but also a set of failures induced by crack propagations as well as tank perforations. The meshes had a characteristic grid cell size similar than that in Mesh 3s. The different tank failures were compared under the ideal hypothesis of the complete symmetric collapse, which assumes that the tank wall suddenly disappears. It is a conservative failure estimation. The most probable failures are the vertical cracks initiated at the bottom of the tank, which propagate following a vertical or horizontal welded line. Focusing on square containments, four failure mechanisms were considered in order to define which one was the more dangerous from the point of view of overtopping. The relative orientations of the failures were also investigated:

1) **Case 1: Total collapse**, in which the fluid was released in all directions.
2) **Case 2: Small hole in the bottom oriented towards the middle of the wall**, the liquid is drained through a small hole. It is usually caused by a broken pipe mouthpiece or a simple perforation by corrosion attack. The break was a square hole of 120 mm × 120 mm placed just above the bund. The ratio between the hole area and the total tank wall area was around 0.65%.
3) **Vertical narrow crack**, initiated at the bottom (1/4 of the tank height) and propagated vertically to the top. The crack was 60 mm wide × 480 mm height and placed just above the bund. The ratio between the crack area and the total tank wall area was around 2.5%. Two orientations were considered: towards the middle of the bund (Case 3) and towards the corner (Case 4).
4) **Horizontal narrow crack**, The crack was $60mm$ height and extended horizontally along 90°. It was placed just above the bund. The ratio between the crack area and the total tank wall area was also 2.5%. Two orientations were considered: towards the middle of the bund (Case 5) and towards the corner (Case 6).

Fig. 5 shows the solutions for the six cases at $t = 0.5$s. Due to symmetry assumptions, a quarter of the overall model was required for solving the total collapse, whereas half of the full geometry was

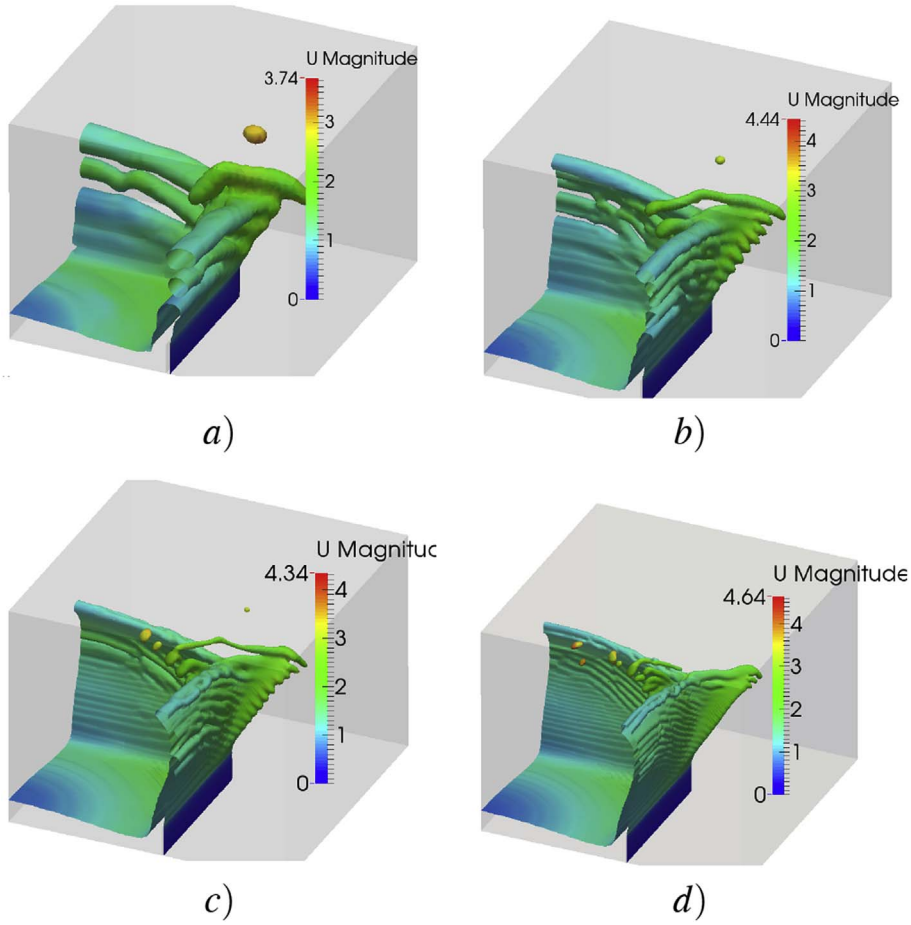

Fig. 3. Square bund test results at t = 0.5s. a): mesh 1. b): mesh 2. c) mesh 3. d) mesh 4.

required for the other cases.

As noted, in the first case all the liquid column collapsed after 0.5s, and a large amount of liquid quickly overcame the bund before the first second. On the other hand, for the small-hole failure (Case 2) the liquid slowly left the tank. The other cases were intermediate situations, in which the rate of release of liquid depended on the size of the crack. For the case of vertical cracks a fraction of the liquid overcame the bund without impacting it. Case 4 was similar to the previous one although the bund was further, thus reducing the amount of liquid overcoming the bund. For cases 5 and 6 (horizontal cracks) the discharge velocity was larger and the drainage increased.

Fig. 5 shows the results for the six cases. The total collapse failure was clearly the worst scenario with an overtopping ratio Q around to 50%, whereas for the other failures the overtopping remained lower than 0.2. The vertical crack oriented in front of the bund (case 3) was the second worst failure Q = 18% and the third worst situation was the horizontal crack oriented towards the corner (case 4), for which Q was around 15%. On the other hand, the overtopping dropped up to 10% both for the horizontal crack oriented towards the front of the wall and the vertical crack oriented towards the corner. Finally, the small hole oriented in front of the wall reached similar inventory loss, although demanding significant more time.

Despite Case 1 represents an extreme situation, it was expected that the consequences were by far the worst. Therefore, case 1 should be considered as a possible event for assessing hazard stored containments under catastrophic failures like this, which have taken place around in the world in last years. In these cases, the tank integrity was completely affected and almost the totality of the stored liquid was delivered in a short time. In fact, real accidents could be even worse than the ideal total collapse in which the liquid is delivered in all directions, whereas in real situations a large fraction, but not the whole tank wall, collapses and the totality of liquid impacts towards part of the bund. Under these circunstances the stress over the bund and breakwaters increases locally. Vertical or horizontal cracks propagating until to reaching structural reinforcements seems to be a much more possible scenario. Hence, engineers should dedicate more efforts to reduce the occurrence of cracks caused by corrosion. They should also estimate the admissible local material loss (minimum tank wall thickness) required to avoid crack propagation based on the hydrostatic loads.

4.3. Shape of the containment

There are only a few possible containment shapes from the technological point of view. The most widely employed are the square and rectangular, although circular containments could be also a choice. In this section, experimental data available in literature (Atherton et al., 2004) for square, circular and rectangular containments were analyzed. Table 4 reports the most important constructive parameters and the results for total collapse of the three above mentioned cases. The distance y is the side length, and d and z are the maximum and minimum distances between the tank and the bund, respectively. For the rectangular case, the side to side dimension was $y \times 2y$. In the three cases, the ratio between the containment capacity and the tank volume V_r was 1.1.

As it can be observed, slightly differences in overtopping for the three configurations were found in accordance with the results from Skitt and Wheeler (1989) and Bentinck and Crow (1991). They observed that the reflected waves interfere each other at the corners of the bund increasing overtopping, which is in agreement with the numerical results showed in Fig. 3. Additionally, they established also that, on a

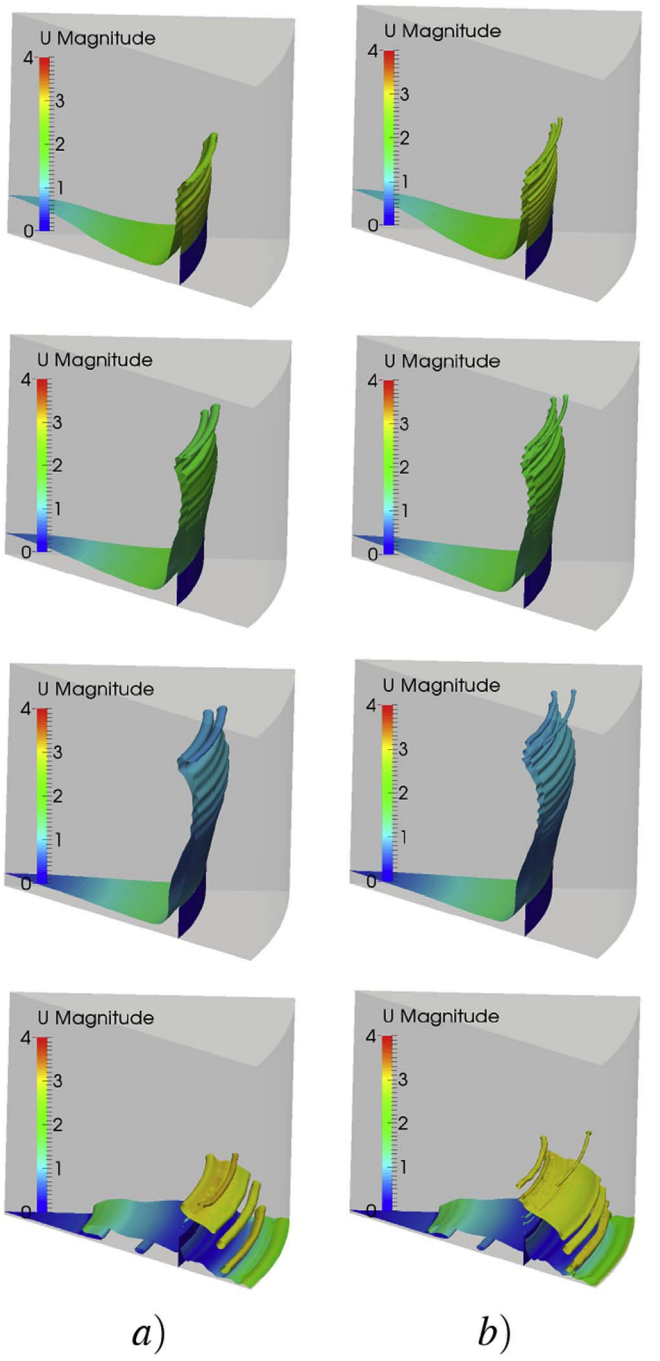

Fig. 4. Circular bund test results (at 0.4,0.5,0.6 and 1*s* for: a) Coarse grid and b) Fine grid.

global level, the degree of overtopping does not differ significantly for plane, circular, or angled (square or octagonal) bunds. It was concluded that for the same bund height h and containment ratio V_r, the containment shape has negligible influence on overtopping. However, it is remarkable that the square containment has 14% more perimeter than the circular one. Hence, the perimeter of the bund could be another factor for selecting containments for isolated tanks.

4.4. Containment capacity ratio R_v

The containment capacity ratio (R_v) can be increased either through increasing the bund height (h), the bund length (y) or also by reducing the tank height (H). In this section, the three possibilities were investigated in order to determine what is the most efficient methodology

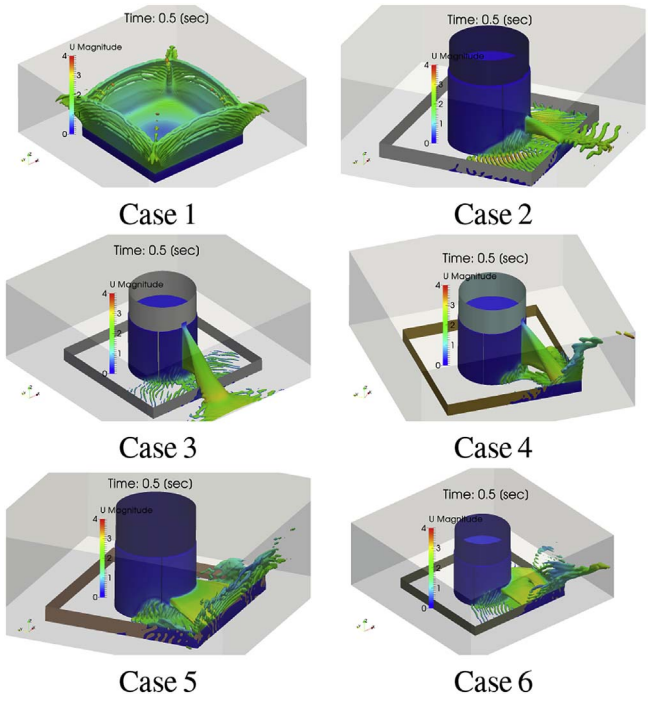

Fig. 5. Solution of the failure modes at $t = 0.5$ sec. Case 1: total collapse. Case 2: small hole at the bottom. Case 3: vertical crack towards the middle of the bund. Case 4: vertical crack towards the corner. Case 5: horizontal crack towards the middle of the bund. Case 6: Horizontal crack towards the corner.

Table 4
Overtopping factor (Q) for total collapse failure for square, rectangular and circular secondary containments.

Shape	y	d	$z(y-R)$	Overtopping
Square (Wall 2 (squ))	624	582	324	48.55
Rectangular (Wall 3(rec))	441	686	141	47.50
Circular (D1(h120))	704	404	404	47.66

in terms of overtopping reduction. The test case was the square containment configuration and the R_v ranged from 1.1 to 1.7. First, the tank height (H) was reduced to accomplish with the different R_v. In a second step, the bund length y was increased keeping constant the bund and tank heights. Finally, the bund height (h) was changed.

Fig. 6 a shows the results for the three cases. As it can be noted, the lowest overtopping was obtained by reducing the tank height H. In this case, an almost linear relation between R_v and Overtopping (Q) was found. On the contrary, the increment of the bund size (y) showed to have slightly influence on Q, which allowed to conclude that the kinetic energy of the falling water column remained almost constant until liquid impacted the bund. In fact, Fig. 6 b shows that the impact pressure became larger while y increased because the fluid was still accelerating. Finally, the last case increasing h led to significant reduction in overtopping, although Q was a bit higher than by reducing H.

Table 5 shows the overtopping factor Q for the three cases. The same results are drawn in Fig. 7 for each one of the studied parameters. As above discussed, the Clarke model in the last column only takes into account the R_v. Therefore, it leads to the same Q for the three analyzed cases, which is contrary to the numerical results. This model was in relative agreement with CFD excepting when the bund length was changed, where the model largely underestimated the overtopping. On the other hand, the Thyer model allowed capturing these dependencies, leading to different estimations depending on the variation of thr bund height h or the tank height H. Furthermore, the model introduces indirectly the parameter y through the bund equivalent radius r_{eq}.

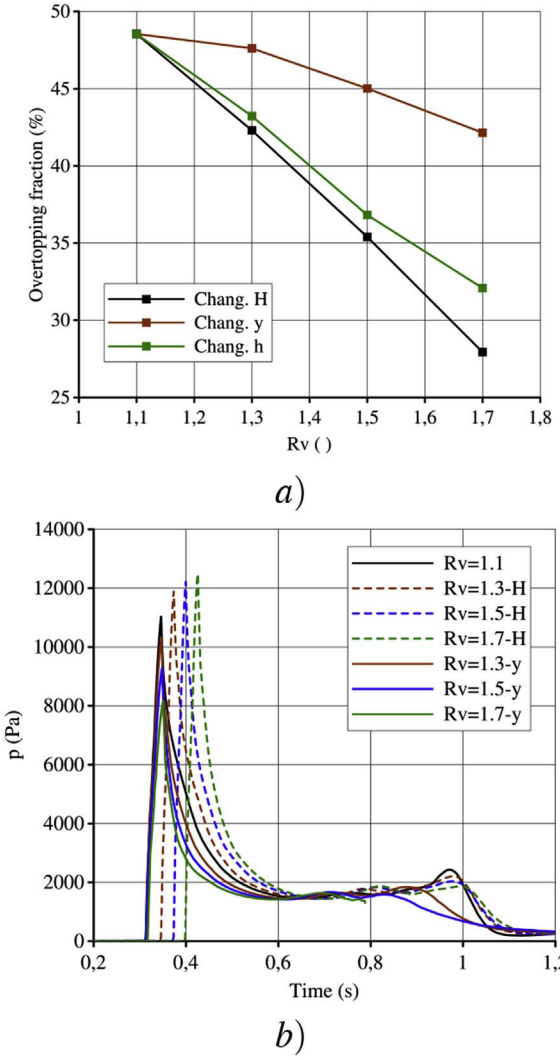

Fig. 6. Failure modes. a): Overtopping factor. b): Pressure at the bund corner.

Table 5
Overtopping factor for different R_v.

R_v –	Change H		Change y		Change h		Clarke
	CFD	Thyer	CFD	Thyer	CFD	Thyer	
1.1	48.55	45.04	48.55	45.04	48.55	45.04	45.99
1.3	42.30	38.74	47.62	44.07	43.23	40.66	39.93
1.5	35.40	33.31	45.02	43.24	36.82	36.89	34.67
1.7	27.93	28.55	42.15	42.52	32.08	33.58	30.10

Therefore, this model led acceptable results in the three cases.

Since the almost linear dependency of Q with h or H, it is easy to calculate the required bund height h for a given overtopping. Therefore, negligible overtopping should be expected by duplicating h. Despite the high improvement, it should be taken into account that the secondary containment should not have any access gate. Then, a high bund would hinder the access for heavy-duty machinery during tank reparations.

4.5. Breakwaters

The use of breakwaters (BW) is scarcely reported in open literature, but it could have a noticeable effect on overtopping control. In the current work, different BW designs were evaluated starting from the square and circular containments before assessed. Five BW were implemented for the most widely known square containments and one BW was evaluated for the circular containment. In all cases being the R_v = 1.1, H = 0.6 m, h = 0.12 m and the BW width equal to 20% of the bund height (h). The first case, called horizontal breakwater ($H - BW$),

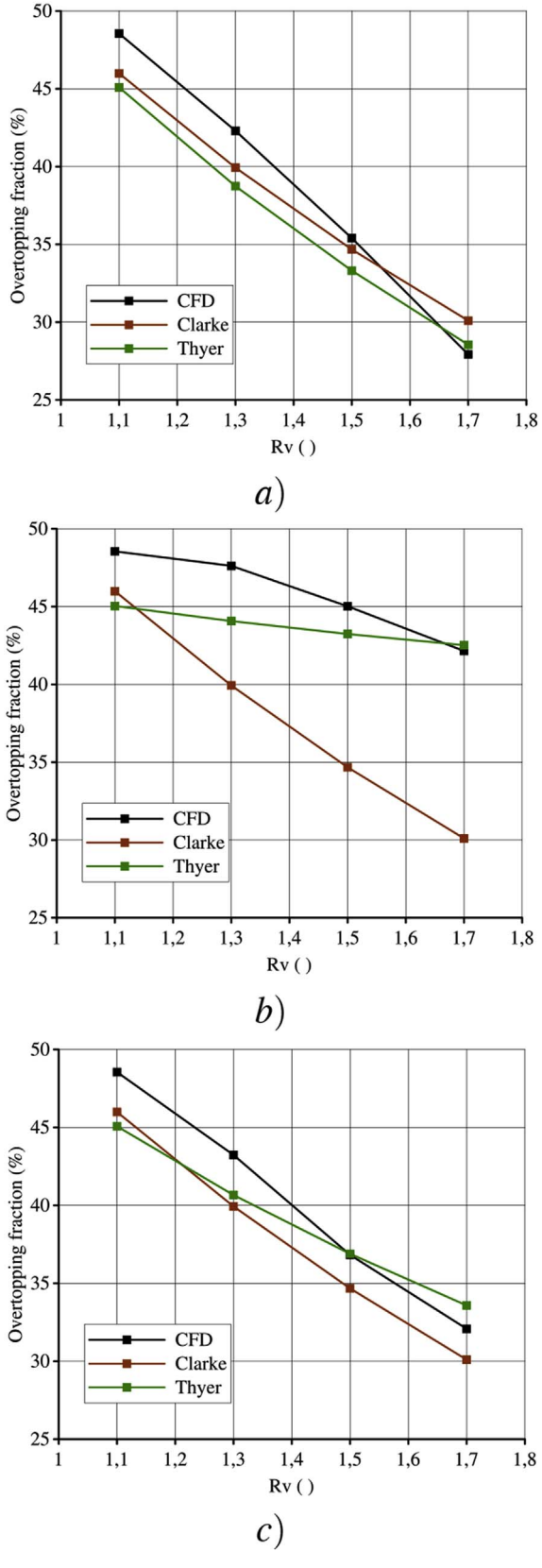

Fig. 7. Overtopping factor: a) Changing H, b) Changing y, c) Changing h.

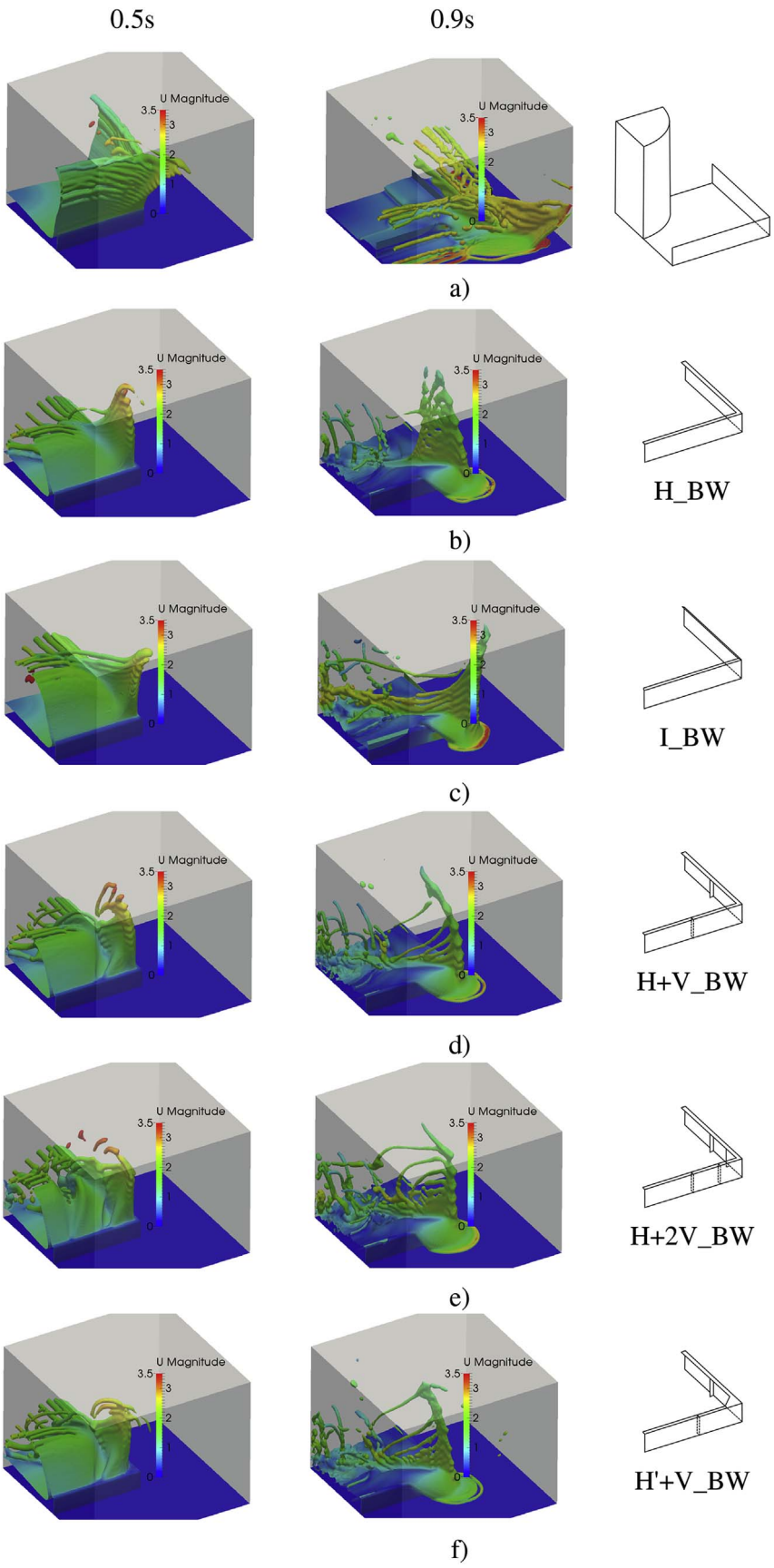

Fig. 8. Results for the breakwater cases at $t = 0.5$s (left pictures) and $t = 0.9$s (right pictures). a): Without BW b): Horizontal BW c) Inclined BW d) Horizontal BW + 1 vertical BW. e) Horizontal BW + 2 vertical BWs f) Horizontal BW + 1 vertical BW and small roof at the corner.

is perhaps the most widely employed, whereas the other cases were novel designs proposed in the current paper. The second design was an inclined breakwater ($I - BW$) aimed to reduce the mechanical loads over the bunds. The third case ($H + V - BW$) incorporated one vertical BW in the middle of the bund. The fourth case ($H + 2 - BW$) incorporated two vertical BWs and the fifth case ($H' + V - BW$) consisted of one vertical BW and a small roof at the corner. These three last cases included vertical breakwaters or partitions in the bund in order to hinder the waves that first impact the bund and subsequently are reflected towards the corners.

Fig. 8 shows schemes of the five designs as well as views of the liquid wave impacting the bund at $t = 0.5$s and $t = 0.9$s. The base case without BW ($NO - BW$) was also included. It can be noted the clear benefit of introducing breakwaters. For the case without BW the liquid leaked over the four bunds causing significant liquid loss. On the contrary, all BWs designs prevented the liquid overtopping across the bunds, although significant liquid escaped through the corners. As it can be noted, the widely used horizontal breakwater ($H - BW$) showed better results than the inclined breakwater ($I - BW$).

Due to the BWs, the waves changed their direction and bounced back into the tank losing some kinetic energy. However, the BWs were not sufficient to completely prevent leakage because the wave front that directly impacted the corner, added to the waves reflected from the lateral bunds, became difficult to control and some leakage remained. According to that, the last three designs were focused on controlling the leakage across the corners. Therefore, the third ($H + VBW$) and forth ($H + 2VBW$) designs introduced vertical breakwaters (partitions) at the bunds to reduce the energy of the reflected flow near the bunds. Additionally, the fith design ($H' + VBW$) locally extended the breakwater around the corner by means of a small roof. These vertical partitions in the bunds reduced the impact of the flow in the corners. Pictures at $t = 0.5$s allow visualizing this effect; despite some liquid was still projected towards the corners, a significant reduction could be observed. Comparing the third and forth designs, the best improvement was achieved through the third one, i.e. using one vertical BW was better than using two of them. Finally, the fifth case ($H' + V - BW$) showed an additional improvement by reducing slightly the leakage through the corner.

To summarize, Table 6 shows the overtopping factor Q, as well as the peak values of the mean pressure P_{avr}, force and momentum. The P_{aver} was calculated as the area average pressure relative to the maximum hydrostatic pressure at the bottom of the bund.

As above mentioned, Q strongly reduced by introducing BWs, although increased largely the mechanical efforts over the bund base as well as at the joint between the bund and the BW mainly due to the additional sudden change on the flow direction after the wave impacted at the BW. As expected, the enhancement of Q was lower by inclining the BW ($Q = 19.61\%$). The vertical BWs placed at the bunds introduced positive effects reducing a bit more the liquid loss. It is noticeable that one vertical BW ($H + V - BW$) had a better effect than two of them ($H + 2V - BW$). Perhaps the explanation could be found in the fact that the reflected wave in the second vertical BW (nearest to the corner) impacted directly over the corner. In addition to the improvement on Q, the vertical BWs should be also seen as an additional structural reinforcement for supporting the high mechanical efforts during a wave impact.

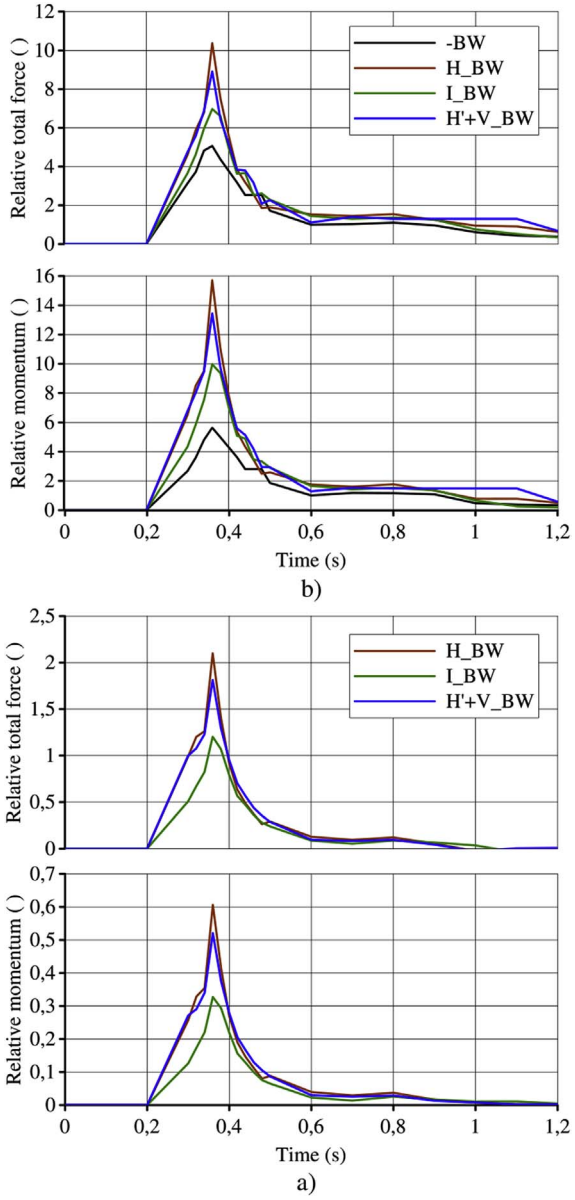

Fig. 9. Breakwater results: Relative total force at the normal direction (top pictures) and momentum (bottom pictures): a) over the top breakwaters. b) Over the bund.

Table 6
Overtopping factor and relative pressure, force and momentum for different breakwaters.

Case	Q	$P_{aver-bund}$	$F_{tot-bund}$	$M_{tot-bund}$	$P_{aver-BW}$	F_{tot-BW}	M_{tot-BW}
Square containment							
NO-BW	48.55	2.5	5.1	5.6	–	–	–
H-BW	12.39	5.2	10.4	15.7	5.3	2.1	0.61
I-BW	19.61	3.5	7.0	9.9	3.0	1.2	0.33
H + V-BW	9.97	4.5	8.9	13.5	4.5	1.8	0.52
H + 2V-BW	10.42	–	–	–	–	–	–
H' + V-BW	8.79	–	–	–	–	–	–
Circular containment							
NO-BW	47.66	3.2	6.4	6.8	–	–	–
H-BW	6.56	5.6	10.7	16.4	5.9	2.36	0.7

The BWs allowed controlling the liquid leakage at the lateral bunds, but were not enough to prevent the overtopping at the corner. In this sense, the last model with the small roof at corner ($H' + V - BW$) reduced a bit more the total overtopping with respect to the model without it ($H + V - BW$).

Fig. 9 shows the relative total forces F_{tot} and momentums M_{tot} over the breakwaters (picture *a*) and the bunds (picture *b*) for the square configuration. The total forces were calculated by integrating the pressure over the bund. The total momentums over the bunds were calculated with respect to the bund base, whereas the momentum over the breakwaters were calculated with respect to the edge joining the bund and the breakwater. Both F_{tot} and M_{tot} were related to the hydrostatic load (F_{ref} and M_{ref}), which takes place under quasi static leakage. For the breakwaters, the same reference load was used because in a quasi static flood the BWs should remain unload.

Regarding the loads over the bunds (Fig. 9,b), the first arrival of the waves was around $t = 0.3$s, but the peak for F_{tot} and M_{tot} took place around $t = 0.38$s. The importance of the dynamic loads was clearly evidenced by the black line corresponding to the case without breakwaters ($NO - BW$). Over the bunds the force peaks were ranged from 5 ($NO - BW$) to more than 10 ($H - BW$) times the expected in hydrostatic conditions. The incorporation of vertical BWs ($H' + V - BW$) reduced the mechanical efforts in the normal direction of the bund. That could be explained by the fact that the vertical BWs reduced the wave impact over the corners. As expected, the use of inclined BWs ($I - BW$) reduced even more the loads, although this design was not as efficient as horizontal BWs to control overtopping. In all cases, the dynamic loads were very high but they lasted for less than 0.4s until the hydrostatic loads were reached.

As for breakwaters (Fig. 9,a), they had to withstand significant loads. For the horizontal BW ($H - BW$) the total force F_{totBW} in the vertical direction reached more than 2 times the total hydrostatic force over all the bund wall. It was a very high effort considering that the BW area was only 20% of the bund area. This force was slightly reduced by introduce vertical BWs ($H' + V - BW$), although the great reduction was achieved by using the inclined BWs (the force was only a half).

Similar behaviors were obtained in the momentums both in the bund and the breakwaters. In these sense, it should be remarked that the $Mtot_{bund}$ became 16 times higher than by hydrostatic load. Moreover, those huge efforts only accounted for the pressure over the bund, but the total momentum at the bund base should also take into account the momentum acting at the BW. Consequently, the total momentum at the bund base could reach up to 18 times the hydrostatic.

Based on these results, the growth of R_v by increasing h along with the use of breakwaters seems to be mandatory. However, it is worthy to note that, despite the significant improvement obtained with the currently studied breakwaters, they did not completely avoid liquid leakage while largely increased the mechanical solicitation over the containment. It should also be consider studying the dynamic loads to avoid the failure of the bund, which could produce the complete spillage of the liquid.

5. Conclusions

In this paper the fast liquid leakages under partial and complete storage tank failures were studied by computational fluid dynamics (CFD). The numerical model was validated against experimental data finding very good fitting. The influence of the containment shape, bund length and height and the use of breakwaters were analyzed in order to enhance the containment efficiency as well as to determine the mechanical loads associated to each design. Novel breakwater configurations were proposed and studied in depth arriving to useful guidelines to build safer containments. The following ideas are highlighted:

CFD is a suitable framework to assist engineers to solve overtopping flow problems, which are mainly governed by inertial forces. The current computational model met errors lower than 3%.

The widely used square containment with 110% capacity ($V_r = 1.1$) without breakwaters was assessed under several possible failure tank events. It was found that the total collapse was by far the most dangerous failure event, for which almost 50% of the total stored liquid was quickly losted in a few seconds. It was also found that the dynamic pressures during the impact -especially at the corners-highly increased the mechanical loads over the bund. The maximum force could reach up to five times the hydrostatic force usually used for structural calculus. Circular, rectangular and square containments (with the same V_r) were found to have very similar overtopping efficiency under total collapse events.

The increment on the bund height h or the reduction of the tank height H led to significant overtopping reduction. A linear dependency between h, H and overtopping was found. On the contrary, the increase of the bund length y, and the consequent increment of the containment enclosure area, had a lower effect.

The incorporation of horizontal breakwaters at the top of the bunds allows reducing overtopping from 50% to less than 13% although largely increasing the dynamic loads (forces and momentums at the bund base). Additionaly, the incorporation of vertical breakwaters aimed to reduce the wave impacts over the corners, reduced overtopping as well as the mechanical loads, also being a good option to enhance the strength of the bund. The best design allows reducing overtopping to less than 9%.

Finally, two analytical models proposed in the literature to estimate overtopping (Clarke and Thyer correlations) were assessed. The simplest model from Clarke only takes into account the containment volume and leads to inaccurate estimations in almost all the cases. On the contrary, the Thyer model considers the most important bund parameters and gives good estimations for bund containments. However, both of them were formulated only for total collapse events and are unable to consider the nature of the tank failure or the use of breakwaters. In view of the results, it is concluded that future work should be dedicated to perform simulations and/or experimental tests to enhance the Thyer correlation to account for the breakwaters effect for different bund configurations varying the main parameters h, H and y. An empirical correlation to estimate the dynamic loads is also paramount.

Acknowledgements

The authors would like to thank Universidad Nacional del Litoral (CAI + D 2011 PJ 500 201101 00015 and CAI + D PI 501 201101 00435), CONICET (PIP 112 201101 00331), ANPCyT (PICT 2013-830) and Universidad Tecnolgica Nacional (PID 4364).

References

Atherton, W., Ash, J., 2007. Review of failures, causes & consequences in the bulk storage industry. In: Proc. 2nd Annu. Liverpool Conf. In Built Environment and Natural Environment.

Atherton, W., Ash, J.W., Alkhaddar, R.M., 2004. The modeling of spills resulting from the catastrophic failure of above ground storage tanks and the development of mitigation. In: 2008 International Oil Spill Conference.

Bentinck, R., Crow, A., 1991. Bund overtopping, 3rd year link project. In: Imperial College, London, and the Health and Safety Executive, Buxton.

Berberovic, E., Roisman, I., Jakirlie, S., Tropea, C., 2010. Computational study of hydrodymanics and heat transfer associated with a liquid drop impacting a hot surface. In: Computational Fluid Dynamics 2010. Springer.

Brackbill, J., Kothe, D.B., Zemach, C., 1992. A continuum method for modeling surface tension. J. Comput. Phys. 100 (2), 335–354.

Chang, J.I., Lin, C.C., 2006. A study of storage tank accidents. J. Loss Prev. Process. Ind. 19 (1), 51–59.

Clark, N., Savery, J., 1993. The catastrophic failure of containment ves- sels, 3rd year link project. In: Imperial College, London, and the Health and Safety Executive, Buxton.

Clark, S., Deaves, D., Lines, I., Henson, L., 2001. Effects of Secondary Containment on Source Team Modelling. HSE CONTRACT RESEARCH REPORT. .

Greenspan, H., Young, R., 1978. Flow over a containment dyke. J. Fluid Mech. 87 (1), 179–192.

Hirt, C., Nichols, B., 1981. Volume of fluid (vof) method for the dynamics of free boundaries. J. Comput. Phys. 39 (2), 201–225.

Ivings, M., Webber, D., 2007. Modelling bund overtopping using a shallow water cfd

model. J. Loss Prev. Process. Ind. 20 (5), 38–44.
Kim, J.S., An, D.H., Lee, S.Y., Lee, B.Y., 2009. A failure analysis of fillet joint cracking in an oil storage tank. J. Loss Prev. Process. Ind. 22 (6), 845–849.
Launder, B., Spalding, D., 1974. The numerical computation of turbulent flows. Comput. Meth. Appl. Mech. Eng. 3.
Law, G., Johnskareng, G., 1994. Containment provisions and overflow of 2-dimensional catastrophic tank failure, 3rd year link project. In: Imperial College, London, Safety Executive, Buxton.
Mesloh, R.E., Marschall, C.W., Buchheit, R.D., Kiefner, J.F., 1988. Battelle determines cause of ashland tank failure. Oil Gas J. 26, 49–54.
Pettitt, G., Waite, P., 2003. Bund design to prevent overtopping. In: Institution of Chemical Engineers, Symposium Series N. 149.
Rusche, H., 2002. Computational Fluid Dynamics of Dispersed Two-phase Flows at High Phase Fractions. Imperial College, London PhD thesis.
Skitt, E., Wheeler, E., 1989. An experimental study of bund over- topping, 3rd year link project. In: Imperial College, London, and the Health and Safety Executive, Buxton.
SreeRaj, R., 2008. Methods of avoiding tank bund overtopping using computational fluid dynamics tool. In: Institution of Chemical Engineers, Symposium Series N. 154.
Thyer, A., Hirst, I., Jagger, S., 2002. Bund overtopping the consequence of catastrophic tank failure. J. Loss Prev. Process. Ind. 15 (5), 357–363.
Ubbink, O., 1997. Numerical Prediction of Two Fluid Systems with Sharp Interphases. Imperial College, London PhD thesis.
Webber, D., Ivings, M., 2010. Modelling bund overtopping using shallow water theory. J. Loss Prev. Process. Ind. 23 (5), 662–667.
Zhang, B., Liu, Y., Zhu, W., Gopalaswami, N., Mannan, S., 2017. Experimental study of bund overtopping caused by a catastrophic failure of tanks. Ind. Eng. Chem. Res. 56, 12227–12235.